Carbon budgets for 1.5 and 2 °C targets lowered by natural wetland and permafrost feedbacks

Edward Comyn-Platt[1]*, Garry Hayman[1], Chris Huntingford[1], Sarah E. Chadburn[2,3], Eleanor J. Burke[4], Anna B. Harper[3], William J. Collins[5], Christopher P. Webber[5], Tom Powell[3], Peter M. Cox[3], Nicola Gedney[6] and Stephen Sitch[3]

1 Centre for Ecology and Hydrology, Wallingford, UK.

2 University of Leeds, Leeds, UK.

3 University of Exeter, Exeter, UK.

4 Met Office Hadley Centre, Exeter, UK.

5 University of Reading, Reading, UK.

6 Met Office Hadley Centre, Joint Centre for Hydrometeorological Research, Wallingford, UK.

*e-mail: edwcom@ceh.ac.uk

Abstract

Global methane emissions from natural wetlands and carbon release from permafrost thaw have a positive feedback on climate, yet are not represented in most state-of-the-art climate models. Furthermore, a fraction of the thawed permafrost carbon is released as methane, enhancing the combined feedback strength. We present simulations with an inverted intermediate complexity climate model, which follows prescribed global warming pathways to stabilization at 1.5 or 2.0 °C above pre-industrial levels by the year 2100, and which incorporates a state-of-the-art global land surface model with updated descriptions of wetland and permafrost carbon release. We demonstrate that the climate feedbacks from those two processes are substantial. Specifically, permissible anthropogenic fossil fuel CO_2 emission budgets are reduced by 9–15% (25–38 GtC) for stabilization at 1.5 °C, and 6–10% (33–52 GtC) for 2.0 °C stabilization. In our simulations these feedback processes respond more quickly at temperatures below 1.5 °C, and the differences between the 1.5 and 2 °C targets are disproportionately small. This key finding holds for transient emission pathways to 2100 and does not account for longer-term implications of these feedback processes. We conclude that natural feedback processes from wetlands and permafrost must be considered in assessments of transient emission pathways to limit global warming.

Introduction

The 2009 meeting of the United Nations Framework Convention on Climate Change (UNFCCC) in Copenhagen formalized the aspiration to stabilize global warming at no more than 2 °C above pre-industrial levels[1]. The subsequent UNFCCC Paris Agreement in 2015 raised the additional possibility of aiming for an even lower upper warming threshold of 1.5 °C (ref. 2). These targets

will require large reductions in anthropogenic greenhouse gas (GHG) emissions, with sustained decreases of ~3% per annum[3,4] and the development of technologies to remove CO_2 from the atmosphere. This is because the equilibrium global warming for current GHG concentrations may already be near 1.5 °C (ref. 5). Given the anticipated difficulty in keeping below the 1.5 °C threshold, two key questions are being asked. First, what are the implications in terms of allowable anthropogenic emissions to keep warming below 1.5 °C rather than 2.0 °C? Second, what is gained climatically or environmentally by keeping below 1.5 °C; that is, are unwelcome climate impacts potentially avoided?

The climate change observed during recent decades has been strongly linked to human influences on atmospheric GHG composition, leading the Fifth IPCC Assessment Report to state: 'it is extremely likely that human influence has been the dominant cause of the observed warming since the mid-20th century'[6]. However atmospheric GHG levels are affected both directly (via anthropogenic GHG emissions) and indirectly by human activity. Indirect effects include climate change-induced adjustments to land–atmosphere and/or ocean–atmosphere GHG exchange fluxes. This was first modelled for the global carbon cycle in ref. 7, where a significant flux of carbon to the atmosphere via increased ecosystem respiration under warming was predicted for a business-as-usual scenario. Similar analyses have been undertaken separately for additional methane (CH_4) release from wetlands[8,9] and additional carbon released from the long-term permafrost store[10,11,12]. The increase in global warming may be underestimated for a prescribed anthropogenic emissions trajectory if these processes are not considered. In reference to policy questions, the anthropogenic fossil fuel emission budgets (AFFEBs) to limit global warming to 1.5 or 2.0 °C may be significantly reduced from current assessments[6,13,14].

This research focuses on two feedback processes that were not included in most models in the fifth phase of the Coupled Model Intercomparison Project (CMIP5)[15] and will only be included in a small fraction of models in the sixth phase (CMIP6). These are the effects of carbon release from the permafrost store as CO_2 and the increased CH_4 emissions from natural wetlands, and the coupling between the two effects where carbon from thawed permafrost is also released as CH_4 (refs [16,17]). These are particularly pertinent issues given that CH_4 has a larger global warming potential (GWP) by equivalent weight than CO_2, and the recent resurgent growth in atmospheric CH_4 (ref. 18).

In contrast to the CMIP5 simulations, which modelled climatic and environmental responses to prescribed atmospheric concentration pathways, the objective here is to quantify the anthropogenic response required to meet a specified global warming target. We develop an inverted form of climate model that follows prescribed temperature trajectories[19] and calculate corresponding AFFEBs[13], including the two aforementioned feedback effects. The modelling framework is based on the coupled Joint UK Land Environment Simulator (JULES[20,21]) and Integrated Model of Global

Effects Of Climatic aNomalies (IMOGEN[22,23]) system (see Methods). The approach taken is generic and may be employed in further research to answer a number of environmental policy-related questions in terms of meeting specified warming thresholds.

Simulations with prescribed trajectories

We use the JULES version 4.8 release, with the addition of a 14-layered soil column for both hydrothermal[24] and carbon[25] dynamics. The JULES configuration includes representations of land use and land-use change (LULUC) and ozone damage on plant stomata to address policy-relevant warming scenarios outside the scope of this paper (see Methods).

The major advancement in the IMOGEN configuration used for this study is the prescription of evolving global temperature trajectories. Following this inverted form (Supplementary Fig. 1b), changes in radiative forcing, ΔQ, are calculated as a function of the time-history of global warming which are then ascribed to compatible atmospheric compositions of GHGs. The anthropogenic contribution to atmospheric CO_2 is calculated whilst taking in to account changes to the land and ocean carbon stores, together with prescription or calculation of non-CO_2 GHGs. Additional IMOGEN enhancements for this analysis include the calculation of atmospheric CH_4 concentration and effective radiative forcing, capturing the climate impacts on CH_4 release from natural wetlands (see Methods).

Critical to our analysis is understanding emission pathways available to stabilize at either 1.5 or 2.0 °C of warming since pre-industrial times. As this will be strongly influenced by anthropogenic perturbation of the climate system to present day, we constrain the historical global temperature (ΔT_G) to the HadCRUT4 observational record[26] and atmospheric composition to the Representative Concentration Pathway (RCP) record[27] for the period 1850–2015. Future projections of the non-CO_2 atmospheric composition is taken from the IMAGE-3.0 implementation of Shared Socioeconomic Pathway (SSP) version 2 under RCP2.6 (SSP2_RCP-2.6_IMAGE)[28] (see Methods).

We select three global warming pathways to stabilization at the 1.5 °C or 2.0 °C targets by 2100 (Supplementary Fig. 1a and SI.2), which are described using the formulation in ref. 19 (see Methods). Two of the considered trajectories reach asymptotes at 1.5 and 2.0 °C from below. The third asymptotes to 1.5 °C after an overshoot to 1.75 °C, representing greater attempts of decarbonization of the atmosphere towards the end of the twenty-first century. The overshoot trajectory allows investigation into hysteresis effects which may have path-dependent effects on temperature stabilization, for example, carbon release due to permafrost thaw.

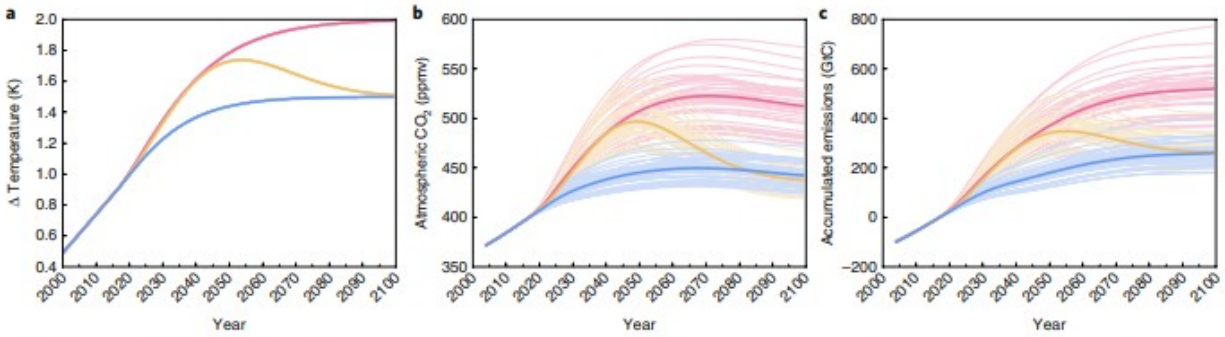

Fig. 1 | Time series for the control model ensemble. a, Temperature pathways. **b**, Simulated atmospheric CO_2 concentrations. **c**, Derived allowable anthropogenic emissions. Blue: 1.5 °C asymptote pathway; yellow: 1.5 °C overshoot pathway; red: 2 °C asymptote pathway. Light lines are individual GCMs, bold lines are the ensemble median, and colours are consistent across the panels.

Feedbacks from natural emissions

Using our control configuration of JULES (that is, with no natural wetland CH_4 nor permafrost carbon feedbacks), we estimate the interquartile range of the AFFEBs for 2015–2100 as 464–568 GtC to meet the 2 °C target, and 227–283 GtC or 227–288 GtC to meet the 1.5 °C target with or without the overshoot, respectively (Fig. 1 and Table 1). The AFFEBs are broadly linear in ΔT_G across the three scenarios, that is, 378–480 GtC °C^{-1} and 421–516 GtC °C^{-1} for the 1.5 and 2 °C scenarios, respectively. These results agree with previous estimates of AFFEBs using different methods[13].

Table 1 | Emission budgets from the factorial experiment and the changes due to the introduction of the feedback processes

		Total anthropogenic fossil fuel CO_2 emissions (GtC)		
		Standard	**Methane feedback**	**Difference**
1.5 °C	Standard	**265** (226–283)	**246** (207–270)	**19.6** (12.1–23.5)[b]
	Permafrostfeedback	**254** (214–271)	**235** (195–257)	**19.9** (12.7–23.7)[b]
	Difference	**11.9** (11.6–12.2)[a]	**12.1** (11.8–12.8)[a]	**31.6** (24.8–35.6) **12.0%** (9.3–14.5%)[c]
1.5 °C overshoot	Standard	**271** (227–288)	**251** (204–275)	**20.8** (12.9–25.2)[b]
	Permafrost feedback	**258** (214–276)	**238** (191–261)	**21.0** (13.4–25.4)[b]
	Difference	**12.5** (12.1–13.0)[a]	**12.7** (12.3–13.4)[a]	**33.5** (25.8–37.8) **12.5%** (9.4–15.1%)[c]
2 °C	Standard	**527** (464–568)	**496** (431–546)	**31.8** (19.3–37.9)[b]
	Permafrost feedback	**514** (451–554)	**483** (418–531)	**32.0** (19.9–38.0)[b]
	Difference	**13.3** (12.8–13.8)[a]	**13.5** (13.0–14.4)[a]	**44.4** (33.4–51.5) **8.5%** (6.4–10.1%)[c]

Cells with no labels[a,b,c] represent the absolute emission budget for the 2015–2100 period. Labelled cells: [a]represent the change due to inclusion of carbon released from the permafrost store; [b]represent the change due to inclusion of an interactive CH_4 scheme; and [c]represent the change due to inclusion of both permafrost and interactive CH_4 feedbacks. Bold values give the climate ensemble median for the 'poor-fen' CH_4 parameterization. Bracketed values represent the interquartile range of the IMOGEN climate ensemble and, in the case of simulations which include the wetland methane feedback, the three temperature sensitivity experiments (that is, the full spread of the boxes in Fig. 3d).

The 2 °C scenario allows close to business-as-usual emissions for the coming decade followed by extensive emission reductions of 3.5–4.1% per year between 2030 and 2100. However, if society were to act more immediately, the AFFEB could be met with year-on-year reductions of 2.2–2.7% from 2020. The 1.5 °C scenario with no overshoot indicates a near immediate peak in annual emissions followed by 3.5–4.3% year-on-year reductions from 2020. Despite the similarity of the AFFEB for the two 1.5 °C scenarios, the

overshoot scenario places larger pressure on future generations. This pathway implies that anthropogenic activities are a net 316–382 GtC source of CO_2 until the early 2050s, then must become a net sink, capturing 81–96 GtC. These estimates go further than previous attempts to quantify AFFEB[13,14] as they provide an AFFEB for each Global Circulation Model (GCM) in the IMOGEN ensemble, and the transient pathway, to meet the specified stabilized temperature.

The role of permafrost thaw in modulating the AFFEB is measured as the amount of carbon that was in the pre-industrial permafrost carbon store that is lost to the atmosphere. We define permafrost as soil layers within grid cells that JULES simulates as perennially frozen. We find that our estimates of present-day permafrost extent and loss rate agree with the models assessed in ref. 11 (Supplementary Fig. 3). Furthermore, a comparison with an observation data set[29] demonstrates that our simulations reproduce a reasonable present-day spatial coverage of permafrost (Supplementary Fig. 4). By 2100, the model ensemble estimates a median 138 Mha loss of permafrost area at 3 m depth for the 1.5 °C asymptote pathway and a median 239 Mha loss for the 2.0 °C pathway (Fig. 2a and Supplementary Table 3). This degradation of permafrost results in an additional 40.0–46.3, 45.6–51.2 and 61.9–72.0 GtC of pre-industrial permafrost carbon that is no longer perennially frozen, relative to 2015, for the three temperature scenarios. Between 20 and 30% of this newly thermally active carbon has been released to the atmosphere, reducing AFFEBs by 11.6–13.8 GtC across the three scenarios (Fig. 2d and Table 1, boxes labelled [a] in the first column). The uncertainty range presented here is the interquartile range of the climate ensemble. We use a model configuration very close to the upper extreme of the process uncertainty presented in ref. 10, so our estimates represent an upper limit to the potential permafrost feedback. Applying the findings of ref. 10 implies that a lower limit to the permafrost feedback would be roughly half of what is presented here (~5–7 GtC).

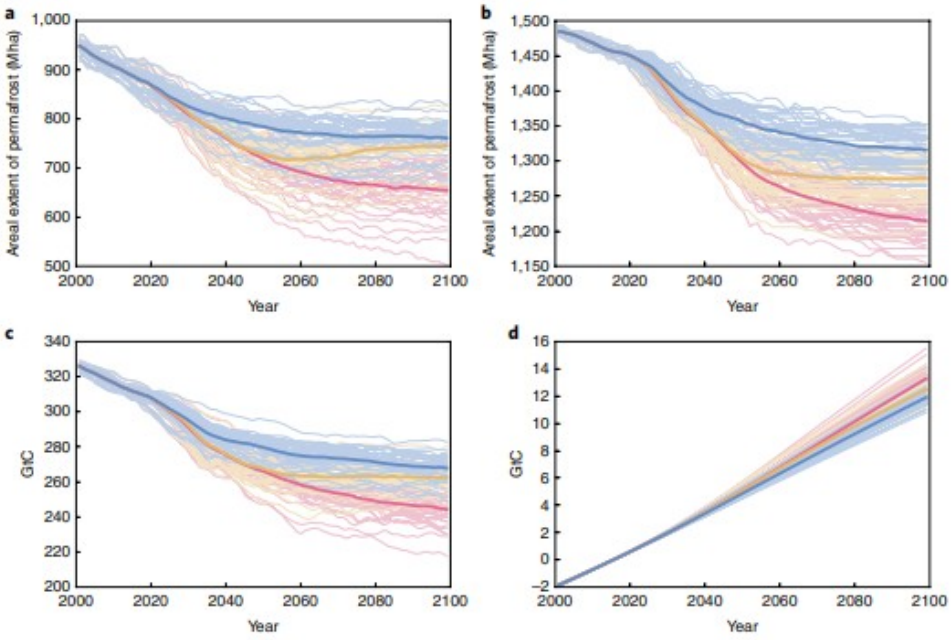

Fig. 2 | Response of the permafrost soil column to warming through the twenty-first century. a, Areal extent of permafrost within the top 1 m of the soil column. **b**, Areal extent of permafrost within the top 3 m of the soil column. **c**, Amount of pre-industrial permafrost carbon still perennially frozen. **d**, Amount of pre-industrial carbon lost to the atmosphere. The reduction in AFFEB for the temperature sensitivity uncertainty ensemble where the horizontal bar represents the median, boxes represent the interquartile range and whiskers represent the maximum and minimum values. Blue: 1.5 °C asymptote pathway; yellow: 1.5 °C overshoot pathway; red: 2 °C asymptote pathway.

The differences in permafrost loss between scenarios appears less than previous estimates[30]. However, our estimates represent a transient snapshot at 2100 and not equilibrium conditions, which will not be met for several centuries. The permafrost is not in equilibrium by 2100; the deeper soil layers in particular show a lagged response to changes in the surface air temperature (Fig. 2a,b). This behaviour is similarly observed in the pre-industrial permafrost carbon stocks, which are still being significantly depleted by 2100 (Fig. 2c,d). The loss rate of pre-industrial permafrost carbon to the atmosphere is still increasing by 2100 as the total pool of soil carbon to respire continues to grow despite stabilization of the surface air temperature. This highlights the timescales involved in permafrost processes and indicates that permafrost thaw will continue to have large implications on anthropogenic emissions into the twenty-second century, even if temperatures have stabilized.

The response of the AFFEB to permafrost thaw is nonlinear with respect to ΔT_G, that is, 19.3–21.7 GtC °C^{-1} for the 1.5 °C scenarios and 11.6–12.5 GtC °C^{-1} for the 2 °C scenario. This implies that the permafrost feedback is faster at lower temperature changes, and keeping temperatures below 1.5 °C, rather than 2 °C, does not make large differences to AFFEBs to 2100. However, this behaviour is primarily a feature of our interest in the AFFEB to 2100, and the additional carbon released in the 2 °C scenario will continue to have implications into the twenty-second century.

The impact of the natural wetland CH_4 feedback on the AFFEBs is the sum of the reduced carbon uptake of the atmosphere, ocean and land due to a higher atmospheric CH_4 concentration. The magnitude and distribution of the JULES natural wetland CH_4 emissions are driven primarily by wetland area and the soil temperature and carbon content (see Methods). Our estimates of wetland extent and zonal distribution for the present day are within the range of state-of-the-art observation data sets[31,32] (Supplementary Fig. 4). To encapsulate a range of methanogenesis process uncertainty we include a temperature sensitivity ensemble by varying Q_{10} in equation (1) (see Methods). We use Q_{10} values calibrated to represent two wetland types identified in ref. 33 ('poor-fen' and 'rich-fen') and a third 'low-Q_{10}', which gives increased importance to high-latitude emissions (see Methods). Our ensemble spread sufficiently describes the magnitude and distribution of present-day CH_4 emissions from natural wetlands according to the models assessed in a recent intercomparison study[34] (Supplementary Fig. 5). However, there is still much uncertainty in natural wetland CH_4 emissions and future work will look to improve our model via more rigorous comparisons with observational data sets.

The global mean atmospheric CH_4 concentrations are increased by 3–9% and 6–15% (w.r.t. the control simulation) when the natural CH_4 feedback is included for the 1.5 and 2 °C targets, respectively (see Fig. 3a for the 'poor-fen' parameterization and Supplementary Fig. 6 for the other parameterizations). The major driver of increased CH_4 emissions is increased soil temperatures, as changes in wetland extent and soil carbon content are not consistent globally (Supplementary Fig. 7). The increased atmospheric CH_4 concentrations imply reduced atmospheric CO_2 concentrations to ensure that simulations follow the prescribed temperature pathway (Fig. 3b). The reduced atmospheric CO_2 concentrations result in reduced CO_2 fertilization of vegetation and a slower oceanic drawdown of CO_2. Additionally, the increased ozone due to increased CH_4 (see Methods) limits productivity further still. The AFFEBs are hence lowered by 12–38 GtC for the full temperature sensitivity ensemble (cells labelled [b] in Table 1 and Fig. 3d).

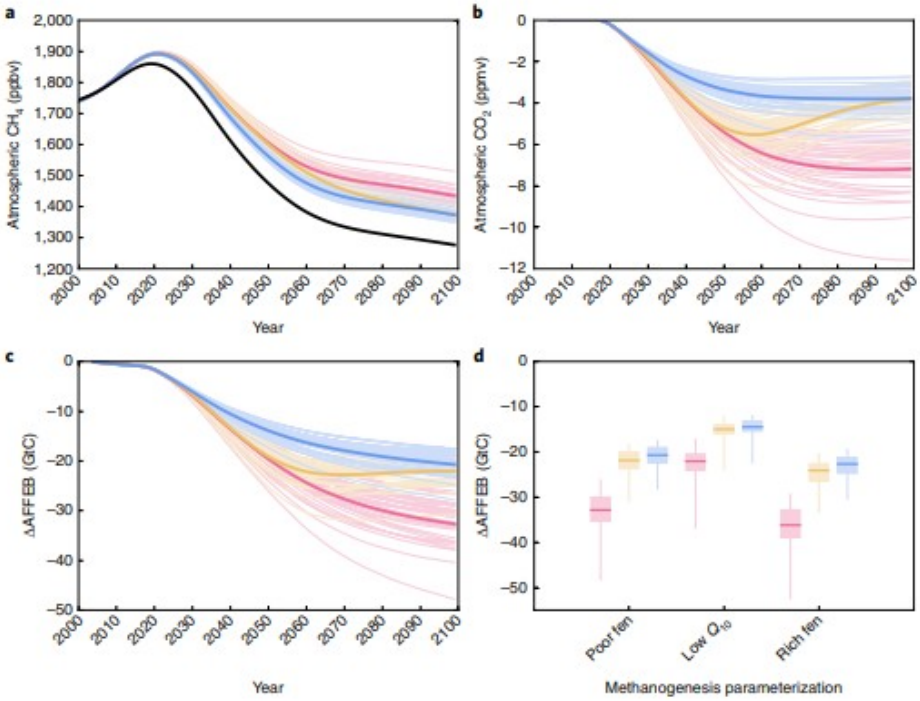

Fig. 3 | Summary results for the natural methane feedback experiment. a, Time series of atmospheric CH_4 when the interactive natural CH_4 is included ('poor-fen' parameterization) for the three temperature pathways. Black line: control simulation atmospheric CH_4. **b**, Reduction in atmospheric CO_2 (from control simulation) to follow the prescribed temperature pathway. **c**, Reduction in anthropogenic fossil fuel emissions due to reduced atmosphere, land and ocean sinks. **d**, Reduction in AFFEB for the temperature sensitivity uncertainty ensemble. Blue: 1.5 °C asymptote pathway; yellow: 1.5 °C overshoot pathway; red: 2 °C asymptote pathway.

Similar to the permafrost feedback, the natural CH_4 feedback is nonlinear with respect to ΔT_G; that is, 20–42 GtC °C^{-1} for the 1.5 °C scenario and 17–34 GtC °C^{-1} for the 2 °C scenario. The effects of the natural CH_4 feedbacks are 50–59% larger for the 2 °C scenario than the 1.5 °C scenarios despite a temperature increase that is 83% larger, from present day. Furthermore, we find that this nonlinear behaviour is consistent for the three temperature sensitivities considered in our uncertainty analysis (Fig. 3d). Therefore, in the context of the natural wetland feedback strength, we conclude that constraining warming to less than 1.5 °C, rather than 2 °C, has a disproportionately small impact on the AFFEB.

The natural CH_4 feedback strength is larger for the 1.5 °C pathway with overshoot in comparison to the 1.5 °C asymptote pathway (Fig. 3d). However, the magnitude of this difference is small (1–2 GtC), hence it is difficult to generalize this behaviour.

Our simulations show little interaction (where thawed permafrost is released as CH_4) between the feedback processes; that is, the difference between the sum of the AFFEB differences and the AFFEB difference from the simulation including both feedback processes is <2 GtC. The amount of CH_4 released from the thawed permafrost carbon is 0.2–0.6 $TgCH_4$ per year, where the upper limit corresponds to the low-Q_{10} parameterization (Supplementary Fig. 8), which gave a greater emphasis to CH_4 emissions from cooler regions (see

Methods). This is ~0.16–0.56% of global CH_4 emissions in 2015, decreasing to ~0.12–0.46% in 2100 (Supplementary Fig. 8b). Similarly, the fraction of permafrost carbon released as CH_4 is 0.15–0.59% (Supplementary Fig. 8). The additional atmospheric CH_4 translates to changes of global atmospheric CO_2 of the order 0.1 ppmv, which has little impact on the absolute atmospheric carbon sink nor the uptake of carbon by the land and ocean. Hence, in the context of our estimates of AFFEBs to meet the UNFCCC targets (200–500 GtC), the interplay of these two feedback schemes is largely negligible. However, our modelling framework does not account for thermokarst lakes created via ground subsidence following permafrost thaw. To provide an estimate of uncertainty regarding this omission we emulate the behaviour offline by linearly increasing the wetland extent in permafrost regions through the twenty-first century, from a factor of 1 in 2000 to a factor of 2 in 2100 (Supplementary Fig. 10). The increased CH_4 emissions reduces the AFFEB by a further 0.8–2.5 GtC. However, we interpret this as an overestimate as the emulation does not consider the reduced aerobic respiration due to increased saturated soil, which has been shown to outweigh the increased CH_4 emissions[16].

1.5 °C versus 2 °C targets

The combined effect of these feedback processes has large implications for AFFEBs: 9.3–15.1% (24.8–37.8 GtC) and 6.4–10.1% (33.4–51.5 GtC) reductions for the 1.5 and 2 °C scenarios from the control runs, respectively (Table 1, cells labelled [c]). In terms of mitigation pathways, this corresponds to 3.6–4.5% year-on-year reductions in anthropogenic emissions beginning in 2020 to meet the 1.5 °C emission budget. To meet the 2 °C warming target, the allowable emissions would require year-on-year reductions of 3.6–4.3% beginning in 2030, or 2.3–2.7% starting in 2020. This represents a 0.1–0.5% increase in reduction rates for the 1.5 °C and a <2% increase in reduction rates for the 2 °C scenario. The 1.5 °C overshoot pathway indicates that total allowable anthropogenic emissions would need to be no more than 291–361 GtC prior to the mid-2050s followed by a removal of 87.1–102 GtC.

We find that to fulfil a 1.5 °C warming threshold with no overshoot, increased CH_4 emissions from natural wetlands reduce the AFFEB between now and 2100 by 7.6–8.3%. Carbon released from the long-term permafrost store reduces the AFFEB by an additional 4.1–5.3%, and the interplay between the two processes a further 0.5–1%. This leaves AFFEBs of 194–257 GtC to 2100, a total reduction of 9.3–14.5%. Allowing for an overshoot to 1.75 °C, but still leading ultimately to 1.5 °C warming, makes little difference to the AFFEB (191–261 GtC to 2100). However, such an eventuality would require significant developments of carbon capture technologies in the second half of the twenty-first century, during which the net anthropogenic contribution to the carbon cycle would have to be a 87–102 GtC sink. The reduction in AFFEB for stabilization at 2.0 °C is, in absolute terms, slightly larger than the reductions required to meet the 1.5 °C target, 33.4–51.5 GtC. However, this is a lower fraction of the AFFEB (6.4–10.1). Our overall findings are that the

natural climate feedbacks considered here are nonlinear with respect to the AFFEB to meet a given temperature target by 2100. Therefore, the roles of the natural CH_4 and permafrost thaw feedback processes become increasingly more important when considering the lower stabilization temperature target of 1.5 °C.

Methods

The JULES model

Model version and configuration

JULES is a process-based land surface model that simulates energy, water and carbon fluxes at the land–atmosphere boundary[20,21]. JULES can be run as a standalone model using given meteorological driving variables or as the land surface component of climate modelling systems of varying degrees of complexity, such as Earth system models (ESMs)[35] or IMOGEN[18]. We use the JULES version 4.8 release with the addition of a 14-layered soil column of over 3 m for both hydrothermal[24] and carbon dynamics[25]. Ref. 25 demonstrated that modelling the soil carbon fluxes as a multilayered scheme improves estimates of soil carbon stocks and net ecosystem exchange. In addition to the vertically discretized respiration and litter input terms, the soil carbon balance also includes a diffusivity term that represents cryoturbation/bioturbation processes. The freeze–thaw processes of cryoturbation are particularly important in cold-permafrost-type soils[10].

The multilayered methanogenesis scheme improves the representation of high-latitude CH_4 emissions (previous studies underestimated production at cold permafrost sites during 'shoulder seasons')[36]. The multilayered scheme allows an insulated subsurface layer of active methanogenesis to continue after the surface has frozen. These model developments not only improve the seasonality of the emissions, but more importantly for this study capture the release of carbon as CH_4 from deep soil layers, including thawed permafrost. The formulation of the multilayered scheme gives the local land–atmosphere CH_4 flux, E_{CH4} (kgC m^{-2} s^{-1}), as

$$E_{\mathrm{CH4}} = k f_{\mathrm{wetl}} \sum_{C_s\,\mathrm{pools}}^{i} \kappa_i \sum_{z=0\mathrm{m}}^{z=3\mathrm{m}} e^{-\gamma z} C_{s_{i,z}} Q_{10} \left(T_{\mathrm{soil}_z}\right)^{0.1\left(T_{\mathrm{soil}_z} - T_0\right)} \qquad (1)$$

where z is the depth in the soil column (in m), i is the soil carbon pool, f_{wetl} (–) is the fraction of wetland area in the grid cell, κ_i (s^{-1}) is the specific respiration rate of each pool (table 8 in ref. 21), C_s (kg m^{-2}) is soil carbon, and T_{soil} (K) is the soil temperature. γ (=0.4 m^{-1}) is a constant that describes the reduced contribution of CH_4 emission at deeper soil layers due to inhibited transport and increased oxidation through the overlying soil layers. This is a simplification; however, previous work that explicitly represented these processes showed little to no improvement compared with in situ observations[37]. The four soil carbon pools (i) in JULES are decomposable plant

material, resistant plant material, microbial biomass, and humus. As JULES is a process based model, the carbon emitted as CH_4 is therefore removed from the soil carbon stock. Furthermore, as described in ref. 38, soil respiration is non-zero in fully saturated soils, so in anaerobic conditions JULES produces CO_2 in addition to CH_4.

f_{wetl} is calculated using the JULES implementation of TOPMODEL[39] as the integral of a normalized gamma distribution of a prescribed topographic index data set[40], $G(\tau)$, between a critical, τ_{crit} (ln(m)), and a maximum, τ_{max} (ln(m)), topographic index, that is,

$$f_{\mathrm{wetl}} = \int_{\tau_{\mathrm{crit}}}^{\tau_{\mathrm{max}}} G(\tau)\,\mathrm{d}\tau \tag{2}$$

τ_{crit} is dependent on the local water table as

$$\tau_{\mathrm{crit}} = \ln\left(\frac{\Psi(0)}{\Psi(\overline{z_{\mathrm{w}}})}\right) + \bar{\tau} \tag{3}$$

where $\Psi(0)$ and $\Psi(\overline{z_{\mathrm{w}}})$ ($\mathrm{m^2\,s^{-1}}$) are the transmissivities of the entire soil column and the soil column below the mean water table depth, $\overline{z_{\mathrm{w}}}$ (m). The τ_{max} limit excludes regions where the water table is sufficiently high enough for stream flow and are therefore assumed to be negligible emitters of CH_4. This is calculated as

$$\tau_{\mathrm{max}} = \tau_{\mathrm{crit}} + \tau_{\mathrm{range}} \tag{4}$$

$\overline{z_{\mathrm{w}}}$ is incrementally updated based on the balance of water flux processes on each JULES time step. When $\overline{z_{\mathrm{w}}}$ is in the deep store (a singular 15 m below the 14 modelled layers) it is updated as the balance between the infiltration water, I_{Deep}, and the baseflow, B_{Deep}, as

$$\rho\theta_{\mathrm{sat}}\frac{\mathrm{d}(\overline{z_{\mathrm{w}}})}{\mathrm{d}t} = I_{\mathrm{Deep}} - B_{\mathrm{Deep}} \tag{5}$$

where ρ is the density of water and θ_{sat} is the saturated volumetric water content. If the deep layer is fully saturated $\overline{z_{\mathrm{w}}}$ is calculated diagnostically to be in the deepest unsaturated model soil layer. The water content of each

layer, j, is updated at each time step as the balance of the vertical flux processes (infiltration I_j and evapotranspiration E_j) and, for layers below $\overline{z_w}$, a horizontal baseflow flux B_j:

$$\Delta z_j \rho \frac{\mathrm{d}(\theta_j)}{\mathrm{d}t} = I_j - E_j - B_j \quad (6)$$

where Δz_j is the thickness and θ_j is the volumetric water content of the jth soil layer. For full details of the process-based JULES hydrology see refs 20,39.

In addition, the JULES configuration includes prescribed LULUC, where land used for agriculture can only grow C3 and C4 grasses to represent crops and pasture. The land-use mask consists of an annual fraction of agricultural land in each grid cell. Historical LULUC is based on the HYDE 3.1 data set[41], and future LULUC is based on SSP2_RCP-2.6_IMAGE[28]. When natural vegetation is converted to managed agricultural land, the removed vegetation carbon is placed into woody product pools that decay at various rates back into the atmosphere[35]. The carbon flux from LULUC is therefore not lost from the system.

We use a JULES configuration including ozone deposition damage to plant stomata, which then affects land–atmosphere CO_2 exchange[42]. JULES requires surface atmospheric ozone concentrations, O_3 (ppb), for the duration of the simulation period (1850–2100). Here, we use two sets of monthly O_3 concentration fields calculated using the HADGEM3-A GA4.0 model for low (1,285 ppbv) and high (2,062 ppbv) global mean atmospheric CH_4 concentrations[43]. We regrid these fields (1.875° × 1.25° horizontal grid) to the spatial grid of IMOGEN-JULES (3.75° × 2.5° horizontal grid). We then linearly interpolate between the respective months in the regridded O_3 fields using the global annual atmospheric CH_4 concentration. The CH_4 concentration is taken from the prescribed SSP2_RCP-2.6_IMAGE plus the natural CH_4 modulation when the interactive scheme is in use.

Wetland CH_4 emission scheme calibration

We calibrate the temperature sensitivity of the multilayered methanogenesis scheme (k and $Q_{10}(T_{soil}) = Q_{10}^{[T_0/T_{soil}]}$ in equation (1)) for each CMIP5 model in the IMOGEN ensemble to ensure the wetland CH_4 production rates match present-day observations[33,34]. Ref. 33 fit observed surface CH_4 fluxes, E_{CH4}, against temperature to equation (7) using data from 71 sites:

$$E_{\mathrm{CH4\_Turetsky}} = A_{\mathrm{Turetsky}} Q_{10\_\mathrm{Turetsky}}^{0.1T_{\mathrm{soil-10cm}}} \quad (7)$$

where $T_{soil\text{-}10cm}$ is the temperature of the top 10 cm of soil.

To capture temperature sensitivity uncertainty we calibrate Q_{10} in equation (1) against equation (7) for two of the wetland types identified in ref. 33 ('Poor-fen' and 'Rich-fen') using the daily output from the JULES simulations at year 2000 for each GCM. We select Q_{10} values that maximize the Pearson's correlation coefficient. k is then calculated such that the global total for year 2000 is 180 $TgCH_4$ to match our assumptions of the atmospheric growth rate of CH_4 in the IMOGEN CH_4 feedback calculations (see IMOGEN description below). We selected the 'Poor-fen' and 'Rich-fen' parameterizations for our ensemble as these gave the best representation of the global distribution of CH_4 emissions when compared with the output from ref. 34 (Supplementary Fig. 9). A 'Bog' parameterization was ruled out as this tended towards unrealistically high tropical emissions, and a 'Swamp' parameterization was ruled out due to the high levels of uncertainty reported in ref. 33. The optimized parameter values are given in Supplementary Table 2. In addition to the two calibrated parameterizations we include a '$lowQ_{10}$' ($Q_{10} = 2.0$, $k = 1.625 \times 10^{-9}$) parameterization, which gave a larger fraction of global emissions to lower-temperature regions (Supplementary Fig. 9).

IMOGEN, EBM inversion and the CMIP5 models selected for its calibration

IMOGEN[23] is a climate-carbon cycle model of intermediate complexity that uses pattern scaling of the seven meteorological variables required to drive JULES. Ref. 23 assumes that changes in local temperature, precipitation, humidity, wind speed, surface shortwave and longwave radiation, and pressure are linear in global warming. Patterns are multiplied by the amount of global warming over land, ΔT_L, to give local monthly predictions of climate change. When using IMOGEN in forward mode, ΔT_L is calculated with an energy balance model (EBM) as a function of the overall changes in radiative forcing, ΔQ ($W\,m^{-2}$). ΔQ is the sum of the atmospheric GHG contributions[44], updated with a yearly time step.

Our simulations include a CH_4 feedback system that captures the climate impacts on CH_4 emissions from natural wetland sources. The approach here follows that of ref. 8 where prescribed CH_4 concentrations, which assume a non-varying natural wetland CH_4 component[28], are perturbed using the anomaly in modelled natural wetland CH_4 emission. To ensure consistency with the observed atmospheric CH_4 growth rate we calibrate our model to produce 180 $TgCH_4$ per year for the year 2000, as detailed in the model calibration description above. The increased/reduced atmospheric CH_4 concentration will have corresponding longer/shorter atmospheric lifetime λ than the prescribed concentration pathway. We account for changes in λ following the formulation and parameterization of ref. 45; that is, $\lambda = 8.4\,yr^{-1}$ for an atmospheric CH_4 concentration of 1,745 ppb. The changes in radiative forcing were calculated using the formulation in ref. [44]. There is large uncertainty in the natural wetland contribution to global CH_4 emissions; for this study we scale to 180 $TgCH_4$ per year, an approximation based on a recent model intercomparison study[34] (Supplementary Fig. 6). Additionally, the effect of increased atmospheric CH_4 concentrations on tropospheric

ozone levels is also taken into account, both in terms of radiative forcing and the impact on surface functioning through stomatal damage (see the description of JULES in the first section of the Methods).

Previous IMOGEN studies[10,23] used 22 of the ESMs involved in CMIP3 (phase 3 of the Coupled Model Intercomparison Project). Here, we update and extend IMOGEN to use ESMs involved in CMIP5. We downloaded CMIP5 data from the mirror database held on the UK JASMIN computer during Autumn 2015. Supplementary Table 1 lists every model for which historical monthly surface temperature fields were available.

The key criteria for inclusion of the output from a given CMIP5 GCM simulation are as follows (see Supplementary Information and Supplementary Table 1):

1. Availability for the internal EBM of surface temperature, top of the atmosphere (TOA) incoming shortwave radiation, outgoing TOA shortwave and longwave radiation

2. Availability of meteorological parameters to drive JULES: surface temperature, precipitation, surface relative humidity, surface downward shortwave radiation, surface downward longwave radiation, surface wind speeds and surface pressure

3. Availability of two RCP scenarios for calibration and testing

EBM inversion

The EBM was inverted such that a change in radiative forcing, ΔQ, is calculated as a function of a change in the global temperature, ΔT_G (K). Re-ordering of equation (10) from Huntingford and Cox[22] gives

$$\Delta Q\,(t) = f\left[\Delta T_{\mathrm{o}}\left[\frac{(1-f)\,\lambda_{\mathrm{l}}\nu}{f}+\lambda_{\mathrm{o}}\right]-\kappa\left.\frac{\partial \Delta T_{\mathrm{o,s}}}{\partial z}\right|_{z=0}\right] \qquad (8)$$

where $\Delta Q(t)$ is the change in radiative forcing ($\mathrm{W\,m^{-2}}$) at time t, f is the fraction of Earth that is ocean, λ_{l} and λ_{o} are the climate sensitivities over land and ocean, respectively ($\mathrm{W\,m^{-2}\,K^{-1}}$), ν is the land–sea contrast and κ is the ocean diffusivity ($\mathrm{W\,m^{-1}\,K^{-1}}$). The values of parameters f, λ_{l}, λ_{o}, ν and κ are unique to each GCM in the ensemble and are listed in Supplementary Table 2.

The change in the depth-dependent ocean temperature (ΔT_{o}) (K) must satisfy the diffusivity equation:

$$c_{\mathrm{p}}\frac{\partial \Delta T_{\mathrm{o,s}}}{\partial t}=\kappa\frac{\partial^2 \Delta T_{\mathrm{o,s}}}{\partial z^2} \qquad (9)$$

where c_p (J K^{-1} m^{-3}) is the specific heat capacity of salt water and z (m) is ocean depth (positive downwards). The change in the global mean surface ocean temperature ($z = 0$) is then calculated from the global temperature ΔT_G as[22]

$$\Delta T_o = \frac{\Delta T_G}{[f + \nu - f\nu]} \tag{10}$$

The global mean land temperature, ΔT_L, required for pattern scaling is calculated as

$$\Delta T_L = \nu \Delta T_o \tag{11}$$

Etminan CO_2 radiative forcing inversion

Etminan et al.[44] present a formulation to calculate the change in radiative forcing, ΔQCO2ΔQCO2, from a given change in the global mean atmospheric CO_2 concentration. There is no exact solution for the inverse of this, that is, to calculate the change in CO_2 for a given ΔQCO2ΔQCO2. We find the solution iteratively using equation (12):

$$CO_{2i+1} = CO_{2REF} \times e^{\left[\frac{\Delta Q_{CO_2}}{a_1 (CO_{2i} - CO_{2REF})^2 + b_1 (CO_{2i} - CO_{2REF}) + c_1 \bar{N} + 5.36}\right]} \tag{12}$$

We assume convergence has occurred if the CO_2 concentration changes by less than 0.001 ppm. The initial CO_2 concentration for the iteration is taken to be the CO_2 concentration for the previous year. We typically find that no more than five iterations are required for a change of 10 ppm from the starting concentration.

Q non-CO_2 calculation

Changes in radiative forcing, ΔQ (W m^{-2}) calculated by the inverted IMOGEN EBM must be ascribed to changes in the atmospheric composition of GHGs. For this simplified description we consider two forcing contributions: the CO_2 forcing ΔQ_{CO2} (W m^{-2}) and the forcing of all other agents, ΔQ_{nonCO2} (W m^{-2}). In the simplest case (not considering interactive CH_4), a prescribed ΔQ_{nonCO2} is removed from ΔQ to give ΔQ_{CO2} as

$$\Delta Q_{CO2} = \Delta Q - \Delta Q_{non\ CO2} \tag{13}$$

The non-CO_2 composition is taken from the SSP2_RCP-2.6_IMAGE pathway[28]. The SSP2_RCP-2.6_IMAGE pathway was chosen as it assumes very high GHG

mitigation and the global warming pathway is reasonably close to the 1.5 or 2.0 °C targets of interest (that is, 1.8 °C by 2100). This prescribed non-CO_2 radiative forcing is subtracted from ΔQ to give the CO_2 radiative forcing ($\Delta Q_{CO2} = \Delta Q - \Delta Q_{non\ CO2}$). The CO_2 concentration is then derived using an iterated inversion of the CO_2 radiative forcing equation in ref. 44. For a given $\Delta Q_{non\ CO2}$, we then estimate the CO_2 concentration iteratively, as described above, using equation (12).

Each of the 34 GCMs that IMOGEN emulates has a different set of EBM parameters: λ_l, λ_o, ν, κ and f. Hence, each GCM has a different ΔQ estimate for a given $\Delta T_G(t)$ pathway. When IMOGEN is driven with a historical record of ΔT_G, the range of ΔQ for the present day (2015) is 1.13 W m^{-2} (Supplementary Fig. 5a). For this work, we require the historical period 1850–2015 to match observations of both ΔT_G and the atmospheric composition for all GCMs. We therefore attribute the spread in ΔQ to uncertainty in $\Delta Q_{non\ CO2}$, in particular the atmospheric aerosol contribution, which has an uncertainty range of −0.5 to −4 W m^{-2} (ref. 6). Given this, and to ensure continuous functions of ΔQ_{CO2} and $\Delta Q_{non\ CO2,}$ we calculated the contributions as

$$\Delta Q_{\mathrm{CO2}}(t) = \begin{cases} \Delta Q_{\mathrm{CO2}}(t)_{\mathrm{SSP}}, & t \le 2015 \\ \Delta Q(t) - \Delta Q_{\mathrm{non\ CO2}}(t), & t > 2015 \end{cases}$$
$$\Delta Q_{\mathrm{non\ CO2}}(t) = \begin{cases} \Delta Q(t) - \Delta Q_{\mathrm{CO2}}(t)_{\mathrm{SSP}}, & t \le 2015 \\ \Delta Q_{\mathrm{non\ CO2}}(t)_{\mathrm{SSP}} + c(\mathrm{GCM}), & t > 2015 \end{cases} \quad (14)$$

where the subscript SSP indicates that the value is sourced from SSP2_RCP-2.6_IMAGE. c (W m^{-2}) is a GCM-specific offset that ensures continuous ΔQ_{CO2} or $\Delta Q_{non\ CO2}$ and was calculated at the transitional year (2015) as

$$c(\mathrm{GCM}) = \Delta Q_{\mathrm{non\ CO2}}(2015) - \Delta Q_{\mathrm{non\ CO2}}(2015)_{\mathrm{SSP}} \quad (15)$$

Supplementary Fig. 5 shows the allocation of the ΔQ and the resultant atmospheric CO_2 concentration pathways for the 2 °C stabilization temperature. We include the GCM-specific 2015 aerosol offsets in Supplementary Table 2.

Temperature profile formulation

Ref. 19 provides a framework to create temperature trajectories based on two parameters that model the efforts of humanity to limit emissions and, if necessary, capture atmospheric carbon, that is,

$$\Delta T(t) = \Delta T_0 + \gamma t - \left(1 - e^{-\mu(t)t}\right)\left[\gamma t - (\Delta T_{\mathrm{Lim}} - \Delta T_0)\right] \quad (16)$$

where $\Delta T(t)$ is the change in temperature from pre-industrial levels at year t, ΔT_0 is the temperature change at a given initial point (in this case $\Delta T_0 = 0.89$ °C for 2015), ΔT_{Lim} is the final prescribed warming limit and

$$\mu(t) = \mu_0 + \mu_1 t$$
$$\gamma = \beta - \mu_0 \left(\Delta T_{\mathrm{Lim}} - \Delta T_0\right) \quad (17)$$

where β (=0.00128) is the current rate of warming, and μ_0 and μ_1 are tuning parameters that describe anthropogenic attempts to stabilize global temperatures[19]. The selected parameterizations of the three trajectories are based on comparisons with CMIP5 simulations for the RCP2.6 scenario (grey lines in Supplementary Fig. 2). The parameter values used for the three profiles selected are also shown in Supplementary Fig. 2.

Data availability

The data that support the findings of this study are available from the corresponding author upon request.

Code availability

JULES is an open-source model and the code branch used in this work is available from the Met Office science repository using the following URL (registration required): https://code.metoffice.gov.uk/trac/jules/browser/main/branches/dev/edwardcomynplatt/vn4.8_1P5_DEGREES?rev=11764.

The parameterizations used herein are also permanently stored on the met-office science repository. Given the complexities in accessing the specific revision and machine configuration required, these will be made available upon request to the corresponding author.

References

1. Copenhagen Accord FCCC/CP/2015/L.9/Rev.1 (UNFCCC, 2009). 2. Adoption of the Paris Agreement FCCC/CP/2015/L.9/Rev.1 (UNFCCC, 2015). 3. Huntingford, C. et al. Te link between a global 2°C warming threshold and emissions in years 2020, 2050 and beyond. Environ. Res. Lett. 7, 014039 (2012). 4. Rogelj, J., McCollum, D. L., Reisinger, A., Meinshausen, M. & Riahi, K. Probabilistic cost estimates for climate change mitigation. Nature 493, 79–83 (2013). 5. Huntingford, C. & Mercado, L. M. High chance that current atmospheric greenhouse concentrations commit to warmings greater than 1.5°C over land. Sci. Rep. 6, 30294 (2016). 6. IPCC Climate Change 2013: Te Physical Science Basis (eds Stocker, T. F. et al.) (Cambridge Univ. Press, 2013). 7. Cox, P. M., Betts, R. A., Jones, C. D., Spall, S. A. & Totterdell, I. J. Acceleration of global warming due to carbon-cycle feedbacks in a coupled climate model. Nature 408, 184–187 (2000). 8. Gedney, N., Cox, P. M. & Huntingford, C. Climate feedback from wetland methane emissions.

Geophys. Res. Lett. 31, L20503 (2004). 9. Shindell, D. T., Walter, B. P. & Faluvegi, G. Impacts of climate change on methane emissions from wetlands. Geophys. Res. Lett. 31, L21202 (2004). 10. Burke, E. J. et al. Quantifying uncertainties of permafrost carbon–climate feedbacks. Biogeosciences 14, 3051 (2017). 11. McGuire, A. D. et al. Variability in the sensitivity among model simulations of permafrost and carbon dynamics in the permafrost region between 1960 and 2009. Glob. Biogeochem. Cycles 30, 1015–1037 (2016). 12. Burke, E. J., Chadburn, S. E., Huntingford, C. & Jones, C. D. CO2 loss by permafrost thawing implies additional emissions reductions to limit warming to 1.5 or 2 °C. Environ. Res. Lett. 13, 024024 (2018). 13. Millar, R. J. et al. Emission budgets and pathways consistent with limiting warming to 1.5 °C. Nat. Geosci. 10, 741–747 (2017). 14. Tokarska, K. B. & Gillett, N. P. Cumulative carbon emissions budgets consistent with 1.5 °C global warming. Nat. Clim. Change 8, 296–299 (2018). 15. Taylor, K. E., Stoufer, R. J. & Meehl, G. A. An overview of CMIP5 and the experiment design. Bull. Am. Meteorol. Soc. 93, 485–498 (2012). 16. Schädel, C. et al. Potential carbon emissions dominated by carbon dioxide from thawed permafrost soils. Nat. Clim. Change 6, 950 (2016). 17. Schuur, E. A. G. et al. Climate change and the permafrost carbon feedback. Nature 520, 171–179 (2015). 18. Crill, P. M. & Tornton, B. F. Whither methane in the IPCC process? Nat. Clim. Change 7, 678 (2017). 19. Huntingford, C. et al. Flexible parameter-sparse global temperature time profles that stabilise at 1.5 and 2.0 °C. Earth Syst. Dynam. 8, 617–626 (2017). 20. Best, M. et al. Te Joint UK Land Environment Simulator (JULES), model description–Part 1: energy and water fuxes. Geosci. Model Dev. 4, 677–699 (2011). 21. Clark, D. et al. Te Joint UK Land Environment Simulator (JULES), model description–Part 2: carbon fuxes and vegetation dynamics. Geosci. Model Dev. 4, 701–722 (2011). 22. Huntingford, C. & Cox, P. M. An analogue model to derive additional climate change scenarios from existing GCM simulations. Clim. Dynam. 16, 575–586 (2000). 23. Huntingford, C. et al. IMOGEN: an intermediate complexity model to evaluate terrestrial impacts of a changing climate. Geosci. Model Dev. 3, 679–687 (2010). 24. Chadburn, S. et al. An improved representation of physical permafrost dynamics in the JULES land-surface model. Geosci. Model Dev. 8, 1493–1508 (2015). 25. Burke, E. J., Chadburn, S. E. & Ekici, A. A vertical representation of soil carbon in the JULES land surface scheme (vn4. 3_permafrost) with a focus on permafrost regions. Geosci. Model Dev. 10, 959–975 (2017). 26. Morice, C. P., Kennedy, J. J., Rayner, N. A. & Jones, P. D. Quantifying uncertainties in global and regional temperature change using an ensemble of observational estimates: the HadCRUT4 data set. J. Geophys. Res. 117, D08101 (2012). 27. Meinshausen, M. et al. Te RCP greenhouse gas concentrations and their extensions from 1765 to 2300. Clim. Change 109, 213 (2011). 28. van Vuuren, D. P. et al. Energy, land-use and greenhouse gas emissions trajectories under a green growth paradigm. Glob. Environ. Change 42, 237–250 (2017). 29. Brown, J., Ferrians, O. Jr, Heginbottom, J. & Melnikov, E. Circum-Arctic Map of Permafrost and Ground-Ice Conditions (National Snow and Ice Data Center, 1998). 30. Chadburn, S. E. et al. An

observation-based constraint on permafrost loss as a function of global warming. Nat. Clim. Change 7, 340–344 (2017). 31. Zhang, B. et al. Methane emissions from global wetlands: an assessment of the uncertainty associated with various wetland extent data sets. Atmos. Environ. 165, 310–321 (2017). 32. Poulter, B. et al. Global wetland contribution to 2000–2012 atmospheric methane growth rate dynamics. Environ. Res. Lett. 12, 094013 (2017). 33. Turetsky, M. R. et al. A synthesis of methane emissions from 71 northern, temperate, and subtropical wetlands. Glob. Change Biol. 20, 2183–2197 (2014). 34. Saunois, M. et al. Te global methane budget 2000–2012. Earth Syst. Sci. Data 8, 697–751 (2016).

Acknowledgements

This work was undertaken as part of the UK Natural Environment Research Council’s programme ‘Understanding the Pathways to and Impacts of a 1.5 °C Rise in Global Temperature’ through grants NE/P015050/1 CLIFFTOP (to E.C.-P., G.H. and S.E.C.), NE/P014909/1, MOC1.5 (to W.J.C., C.P.W., C.H., P.M.C. and S.S.) and NE/P014941/1 CLUES (to A.B.H., P.M.C. and T.P.). The authors also acknowledge support for E.J.B. and N.G. through the Joint UK BEIS/Defra Met Office Hadley Centre Climate Programme (GA01101), E.J.B. through CRESCENDO (EU project 641816), A.B.H. through an EPSRC Fellowship ‘Negative Emissions and the Food–Energy–Water Nexus’ (EP/N030141/1), and C.H. through CEH National Capability Funding. The authors also acknowledge the wetland extent data products provided by B. Zhang of Auburn University and B. Poulter of the NASA Goddard Space Flight Center.